Journal of Materials Chemistry B

ROYAL SOCIETY OF CHEMISTRY

PAPER

View Article Online
View Journal | View Issue

Cite this: J. Mater. Chem. B, 2025, 13, 3032

A versatile two-light mode triggered system for highly localized sequential release of reactive oxygen species and conjugated drugs from mesoporous organosilica particles†

Hannah Bronner,[a] Katharina Doll-Nikutta,[bc] Sören Donath,[cd] Nina Ehlert,[ac] Yaşar Krysiak,[a] Alexander Heisterkamp,[cd] Meike Stiesch,[bc] Stefan Kalies*[cd] and Sebastian Polarz*[a]

The increasing prevalence of antimicrobial resistance and adverse effects of systemic treatments calls for urgent reevaluation of current methods that rely on excessive, uncontrolled drug administration. In recent years triggerable systems have emerged as promising alternatives, enabling time-controlled and localized drug release, which are only activated if necessary. Light is an obvious candidate as an external trigger, since it allows for localized activation, is non-invasive and its wavelength and intensity can be tailored to fit the demands of the drug release system. Such localized and triggered systems minimize off-target effects and undesired exposure, making it a promising tool for combating health threats such as antimicrobial resistance. However, the limited tissue penetration of visible light significantly limits the applicability of this concept *in vivo*. Here, we introduce an innovative triggerable drug release system, based on mono-, bi-, and tri-functionalized mesoporous organosilica particles (MOPs). The limited tissue penetration is addressed by an advanced trigger system featuring two-photon absorption. Two-photon absorption enables utilization of near-infrared (NIR) light as a trigger, which is known to exhibit an enhanced penetration depth. The particles are designed to release reactive oxygen species (ROS) upon NIR irradiation and undergo Förster resonance energy transfer (FRET) to a ROS producing dye. Moreover, by oxidative cleavage, an additional therapeutic agent is released in a cascade reaction, enhancing the system's effectiveness. The ROS release is microscopically demonstrated *in situ* and, for the first time, release of a fluorescent compound (therapeutic agent) in a cascade reaction is observed in real-time, providing valuable insights into the behavior and performance of our particles. This novel sequential dual-release platform for light-triggered therapeutic delivery has great potential for advanced therapeutic applications in both superficial and deep tissue treatments.

Received 4th December 2024,
Accepted 20th January 2025

DOI: 10.1039/d4tb02691h

rsc.li/materials-b

Introduction

Conventional treatments, such as antibiotics, are confronted with significant challenges due to high systemic exposure, affecting not only the intended targets but also healthy cells or non-target microbes. This broad exposure increases side effects and, in the case of antibiotics, accelerates bacterial antimicrobial resistance (AMR), which is associated with more than 5 million deaths.[1] It is thus evident that a rethinking of systemic treatment is imperative. The development of smart materials that can be activated reliably when needed, yet remain harmless when not required, represents an essential solution. Given the potential for controlling the spatio-temporal release through the intensity and duration of irradiation, light emerges as a promising external trigger for biomedical drug-release systems. Light can be used to trigger chemical reactions and for example release active compounds through the cleavage of a photolabile cross-linker.[2] However, it is even more desirable to use light as a catalyst for a sustainable reaction. In this regard, the concept of (antibacterial) photodynamic therapy (PDT) has attracted considerable interest in recent years. A photosensitizer

[a] Institute of Inorganic Chemistry, Leibniz University Hannover, Callinstraße 3-9, 30167 Hannover, Germany. E-mail: sebastian.polarz@aca.uni-hannover.de
[b] Department of Prosthetic Dentistry and Biomedical Materials Science, Hannover Medical School, Carl-Neuberg-Str. 1, 30625 Hannover, Germany
[c] Lower Saxony Centre for Biomedical Engineering, Implant Research and Development (NIFE), Stadtfelddamm 34, 30625 Hannover, Germany. E-mail: kalies@iqo.uni-hannover.de
[d] Institute of Quantum Optics, Leibniz University Hannover, Welfengarten 1, 30167 Hannover, Germany

† Electronic supplementary information (ESI) available. See DOI: https://doi.org/10.1039/d4tb02691h

(PS), which may be a semiconductor or a chromophore, is irradiated with the light of appropriate wavelength, whereby the photogenerated charge carrier reacts with oxygen or water molecules to form reactive oxygen species (ROS).[3] ROS, including superoxide ($O_2^{\bullet -}$), singlet oxygen ($^1O_2$), the hydroxyl radical ($HO^{\bullet}$), and hydrogen peroxide (H_2O_2), show remarkable efficacy against bacteria that possess limited intrinsic defenses due to low specificity and high chemical potency of ROS. By incorporation of PSs in materials, their disadvantages of low water-solubility and tendency for aggregation, as well as their limited photostability are improved.[4]

Even though particle-based PDT improves its shortcomings, the short lifetime of ROS still limits the effectiveness of PDT. Therefore, synergistic concepts that simultaneously release ROS and a second compound have proven to be beneficial.[5] As the efficacy of antibiotics and materials that release antibiotics is a topic of debate due to previously named arguments, the use of alternative active molecules is necessary. Another category of active ingredients that can be employed for the prevention of colonization and biofilm formation are essential oils (EOs).[6–8] Amongst them, thymol, a natural monoterpenoid with relatively low toxicity for humans, has shown anti-microbial activity based on its disruption of bacterial cell membranes.[9] Thymol has also been identified as a way of reducing bacteria biofilm formation in subinhibitory concentrations.[10] As thymol is only slightly soluble in water at neutral pH and is also highly volatile, it requires heterogeneous support and gradual release.[11,12]

A further critical limitation of PDT arises upon closer examination of its trigger *via* irradiation. PDT is most effective in cell culture experiments, where the materials can be subjected to high light doses of ultraviolet (UV) or visible (VIS) light. However, this is not an applicable approach in deep biological tissue, including the skin, which is not translucent for UV-VIS irradiation.[13] The near-infrared window where light has its maximum depth of tissue penetration, also known as the therapeutic window, ranges from 650 nm to 950 nm.[14] Conventional PSs, on the other hand, require more energy to catalyze the photoreduction of oxygen than can be provided by low-energy light in the therapeutic window. Therefore, ROS-producing PDT systems working with near-infrared (NIR) light are highly desired and are another major challenge for the trigger system. One solution to this obstacle is the use of non-linear excitation instead of conventional light.[15,16] Two-photon excitation is a non-invasive technique that uses a focused laser beam to provide the required energy through the simultaneous excitation of two photons with less than the necessary energy (see the Jablonski diagram in Scheme S1, ESI†).[17]

The objective of the current paper is to achieve two milestones: (i) based on our previous papers on mesoporous organosilica particles (MOPs) capable of ROS production,[18,19] a novel drug-delivery system will be developed that combines ROS production with a sequential thymol release (Fig. 1b). The sequential character is realized using an oxidatively cleavable linker.[13,20] (ii) After showing this route, we will further describe

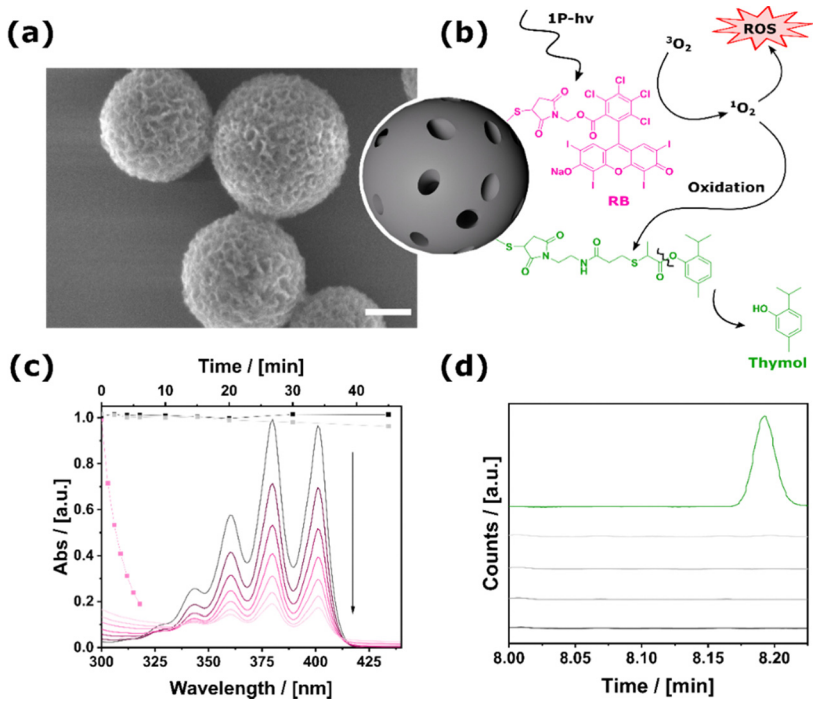

Fig. 1 (a) SEM micrograph of MOPs (scale bar represents 100 nm). (b) Schematic representation of MOPs for ROS production and sequential thymol cleavage. (c) ABDA (9,10-anthracenediyl-bis(methylene)dimalonic acid) assay of MOPs-RB under irradiation with green LED light confirming ROS-production (black: t = 0 min to light pink: t = 6 min, a measurement was taken every minute). Arrow indicating the decomposition of ABDA. Time-dependent decomposition of ABDA under different conditions: irradiation with green LED (pink dots), kept in the dark (black dots), and kept in the daylight (grey dots). (d) GC-MS chromatogram of MOPs-Thymol that were kept in the dark (black: t = 0 min, dark grey: t = 20 min, middle grey: t = 4 h, light grey: t = 24 h, green: signal of free thymol measured as a reference). The intensity is normalized and referred to an internal standard.

the evolvement of our system for highly localized application in deep tissue using nonlinear two-photon excitation.

Results and discussion

Bifunctional materials activated by VIS light irradiation for dual ROS and small molecule release

Initially, the carrier material was synthesized. This was achieved by converting the sol–gel precursor 1,5-bis-tri(isopropoxysilyl)-benzene-3-thiol to mesoporous thiol-containing particles (MOPs-SH) *via* a template-based approach (see the experimental section given in the ESI,† Section S1).[21,22] Using base-catalyzed Thiol–Michael addition any desired functional molecule with an appropriate maleimide compound can be bound to the MOPs-SH (detailed description of the molecular synthesis can be found in the experimental section of the ESI,† Section S1). Firstly, we describe the synthesis and properties of mono-functional particles and then successively increase the number of functional groups attached to the surface of the particles.

Section S2.1 of the ESI† provides a detailed account of the MOPs containing Rose-Bengal (MOPs-RB) and their characterization, with particular emphasis on the production of ROS. For MOPs-RB, the amount of immobilized Rose Bengal could be determined to 96.1 μg per mg particles. ROS generation was probed by monitoring the decomposition of ABDA (9,10-anthracenediyl-bis(methylene)dimalonic acid) using UV-VIS spectroscopy (Fig. 1c). As expected, the system is inactive when the particles are kept in the dark, and also exposure to ambient light is not sufficient for ROS production. However, irradiation with green LEDs at λ_{max} = 530 nm resulted in the fast production of ROS.

For the synthesis of MOPs-Thymol, the respective maleimide compound, which contains an oxolabile linker (Fig. 1b), was reacted with MOPs-SH (see the ESI,† Section S1, 2.2, for details). It was determined that 68.6 μg of thymol could be attached to each mg of the particle. This sample was prepared to ensure that the phenolic ester group between thymol and the maleimide is stable under non-oxidative conditions, respectively, in the dark and at physiological pH. As depicted in Fig. 1d, the data demonstrates that there was no significant release of thymol following an incubation period of 24 hours. Extending the storage time to 35 days indicated long-term stability and no unwanted leakage from MOPs-Thymol was observed (see the ESI,† Section S2.2).

Depending on the ratio of the two different functional maleimides in the reaction solution, a whole range of samples MOPs-RB^m-ROS-Thymol^n can be realized (see Fig. 2a). The synthesized samples vary from ≈ 1 : 3 to 1 : 38 (Fig. 2a; Section S1, 2.3, ESI†). In the absence of light, there is no ROS production and, consequently, no cleavage of thymol. Fig. 2b shows the light-induced generation of ROS probed *via* the ABDA assay. The more RB the sample contains, the faster the decomposition of ABDA and therefore the higher the ROS generation. The oxidative ester cleavage reaction has the effect of dampening the rate of ROS production, which consequently results in a longer time period being required to reach a high level when a greater quantity of thymol is attached to the bifunctional MOPs. This and the overall lower amount of immobilized RB explains the rate decrease compared to MOPs-RB (Fig. 1c) for all MOPs-RB^m-ROS-Thymol^n samples. Nevertheless, the particles will have an impact on potential targets through released and excess ROS.

To prove the efficient release of thymol, the formation of free thymol was analyzed by taking aliquots of the suspension after irradiation; the particles were filtered off, followed by GC-MS (gas chromatography mass-spectrometry) measurements of the supernatant. The original GC measurements, showing the results for the individual time points, can be found in Section S2.3 in the ESI.† The time-dependent thymol release is shown for different MOPs-RB^m-ROS-Thymol^n in Fig. 2c. For the binary MOPs, a significant release of thymol is observed, increasing rapidly within the first 20 min of irradiation to a total of nearly 60 μM. It is reasonable that the amount of free thymol scales to the number of molecules attached to MOPs.

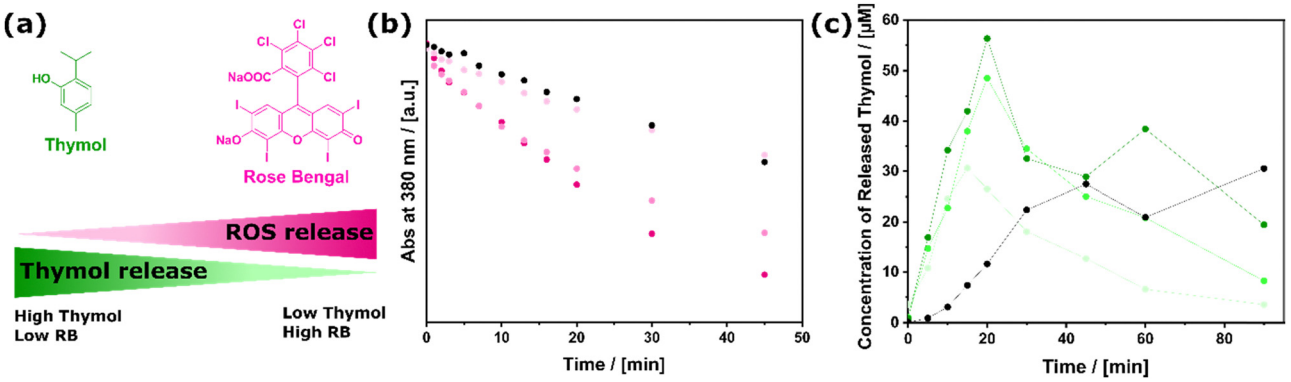

Fig. 2 Bifunctional MOPs-RB^m-ROS-Thymol^n system. (a) Color-coding of samples with varying ratios of immobilized thymol and RB used in the ROS detection and thymol release assay dark green and light pink stand for samples with high amount of immobilized thymol and low amount of RB and *vice versa* (for exact ratios see Section S2.3, ESI†). (b) ROS production of binary MOPs-RB-Thymol: with more RB on MOPs, more ROS is produced (light pink to dark pink). Black: sample of mixed MOPs-RB and MOPs-Thymol. (c) Thymol release of binary MOPs-RB-Thymol: with more thymol on MOPs, more thymol is released (light green to dark green). Black: sample of mixed MOPs-RB and MOPs-Thymol.

The emergence of a maximum at $t \leq 20$ min seems surprising at first glance. However, the ROS-mediated oxidation of thymol can explain the decrease in the concentration of free thymol to thymoquinone at higher times. The latter result indicates that it is highly important to control both the ratio $n:m$ and the duration of light exposure. Furthermore, the immobilization of both functions on one particle had a synergistic effect: when compared to a mixture of the mono-functionalized particles (MOPs-RB + MOPs-Thymol), the bifunctional system showed an earlier and more efficient release (see Fig. 2c, black dots). This can be explained by the shorter distance between the ROS producer and the oxolabile linker on a single particle, in comparison to the interparticular distance. The results prove the feasibility of the light-triggered dual release of ROS and thymol (Fig. 1b).

To further address whether MOPs-RB-ROS-Thymol exhibits advantageous antibacterial properties over the mono-functional nanoparticles in a biological context, preliminary experiments were conducted to test the antibacterial activity against *Staphylococcus aureus*, a commensal skin bacterium highly associated with nosocomial infections. A benefit of light-activated MOPs-RB-Thymol was only observed for a concentration of 0.25 mg ml^{-1}. The detailed description of the experiments and the corresponding results can be found in Section S1.4 and S2.4 in the ESI.† In the future, a more detailed biology-focused analysis will

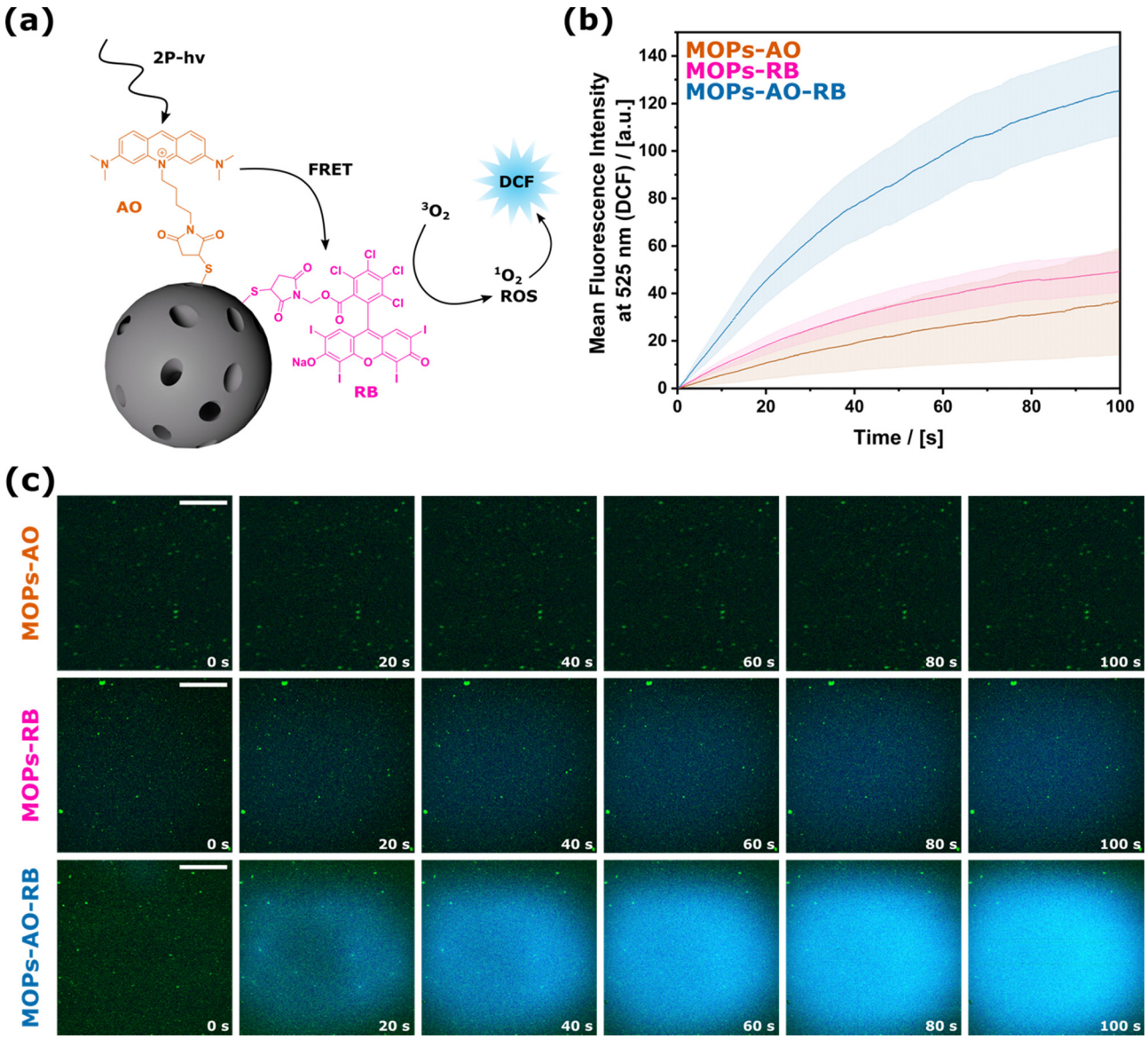

Fig. 3 (a) Schematic structure of binary MOPs-AO-RB used in 2-PE ROS production. Irradiation starts the cascade reactions: (1) excitation of Acridine Orange (AO), (2) FRET transfer of the energy to RB, which (3) transfers its energy to excite triplet oxygen to singlet oxygen (ROS production). (b) Increasing mean fluorescence intensity that equals the ROS production (monitored by the reaction of non-fluorescent DCFH with ROS and forming fluorescent $DCFH_2$) of MOPs-AO (brown), MOPs-RB (pink) and MOPs-AO-RB (blue) by averaging the fluorescence intensity of 8 individual experiments (error bars show the standard deviation) and (c) exemplary time-resolved ROS production of MOP materials monitored using fluorescence microscopy. Particles are pseudo-colored in green and the DCF signal pseudo-colored in blue. Scale bar corresponds to 50 μm.

be necessary based on this initial determination of the applicability and initial parameter evaluation.

Materials activated by two-photon excitation for highly localized ROS production and potential deep-tissue penetration

As the drug delivery system described up to this point can only be operated using VIS light, we aimed to evolve the materials further so that they could function with NIR light by making use of two-photon excitation (2-PE) processes. Even though the absorption probability of 2-photon irradiation is lower than irradiation with linear light, the advantage is that deep penetration into biological tissue can be achieved with NIR wavelengths, which enables confining effects to the focal volume. The general concept is shown in Fig. 3a. Light absorption occurs by a two-photon absorbing dye, which activates RB as the established producer of ROS *via* Förster resonance energy transfer (FRET).[23,24] FRET describes a non-radiative, physical process that transfers energy from a donor (Acridine Orange, AO) to an acceptor (RB) through dipole–dipole interactions. For efficient energy transfer, the distance between the two dyes must be less than 10 nm, and there must be a significant spectral overlap between the donor's emission and the acceptor's absorption.[25,26] In our system, the process unfolds as follows: incoming photons excite electrons of AO from its ground state to an excited state. Due to the proximity of RB and the substantial spectral overlap (see UV-Vis spectra in Fig. 4b), AO bypasses photon emission and instead transfers its energy to RB *via* dipole–dipole coupling. The excited singlet state transitions to a triplet state through intersystem crossing. The excited RB then returns to its ground state by transferring the energy to an oxygen molecule, generating ROS. The corresponding schematic energy diagrams can be found in Scheme S1 in the ESI.† AO was selected as the two-photon absorber because of the large spectral overlap with RB (see Fig. 4b).[27–29] In the previous section, we identified RB as

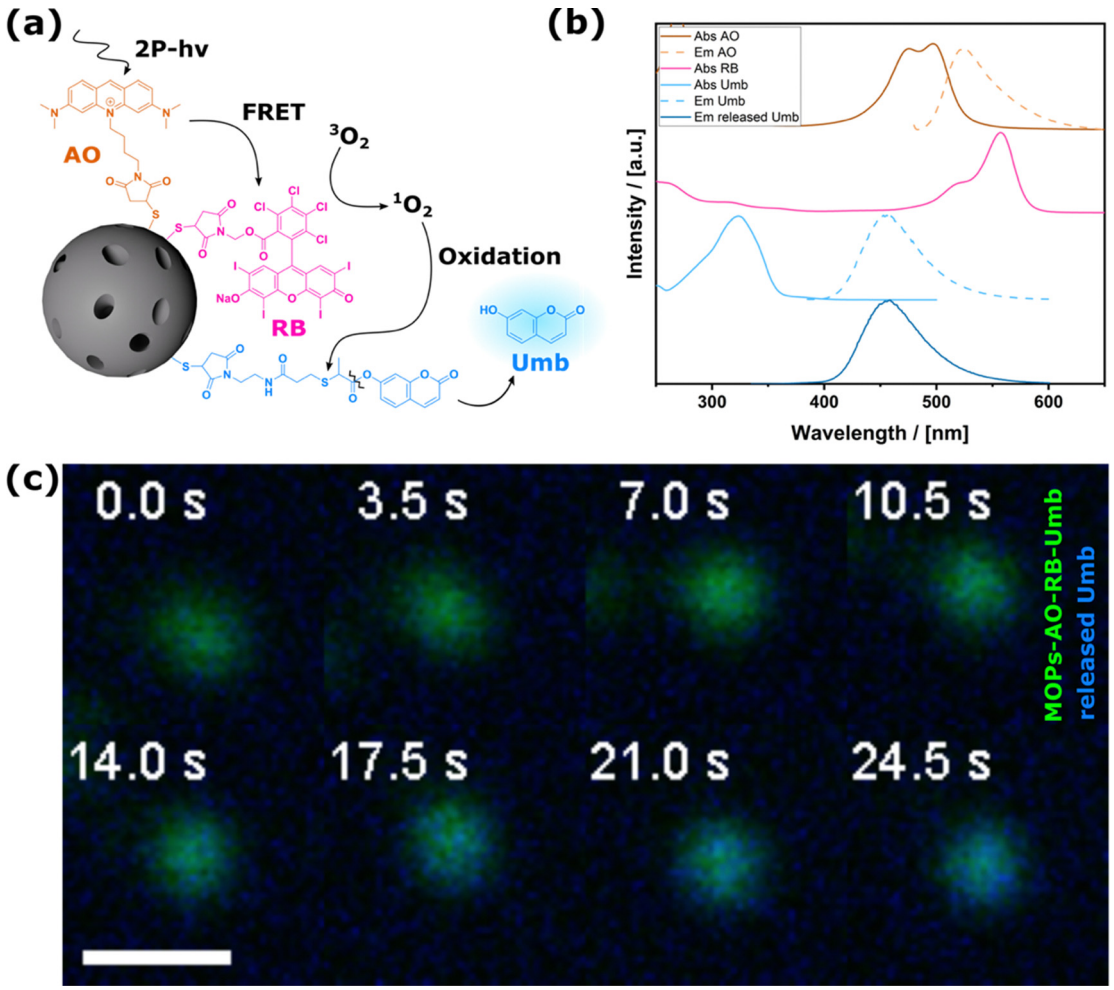

Fig. 4 (a) Schematic structure and cascade reaction of ternary MOPs-AO-RB-Umb which release umbelliferone monitored by *in situ* fluorescence microscopy. (b) Absorption and emission spectra of Acridine Orange (modified for the click reaction), Rose Bengal (modified for the click reaction), umbelliferone, and fluorescence emission of released umbelliferone from MOPs-AO-RB-Umb. The spectral overlap of AO emission and RB absorption is between approx. 510 and 590 nm. (c) *In situ* detection of released umbelliferone (blue) from MOPs-AO-RB-Umb (pseudo-colored in green) under 2-PE irradiation. Scale bar corresponds to 500 nm.

an efficient photosensitizer under VIS irradiation, which prompted us to examine its performance under NIR wavelengths. The attachment of AO *via* the described maleimide – thiol click chemistry (see the Experimental part S1 in the ESI† for details) leads to MOPs-AO^m-RB^n. The optical properties of materials differing in $n:m$ were recorded, and even though the FRET efficiency for all samples was higher than 85%, the optimum for the FRET process was observed for an equimolar amount of AO to RB. A comprehensive account of the calculations and supplementary clarifications regarding the FRET process, together with the associated data, can be found in the ESI† Section S2.5. ROS production by MOPs-RB, MOPs-AO, and MOPs-AO-RB under 2-PE irradiation was investigated using the *in situ* oxidation of $DCFH_2$ (2′,7′-dichlorodihydrofluorescein, a non-fluorescent probe) to DCF (2′,7′-dichlorofluorescein, a fluorescent one), which is widely used to observe intercellular ROS levels.[30,31] As expected, particles that are only functionalized with either of the dyes (MOPs-AO or MOPs-RB) resulted in low oxidized DCF (see Fig. 3b and c).

Combining both functionalizations (MOPs-AO-RB) led to the synergistic enhancement of ROS production. A closer look at the *in situ* observation (see Movies S1, ESI†) of the first few seconds is particularly impressive, as it was possible to see exactly how the ROS is generated near individual particles or particle agglomerates. Even though the combination of FRET and ROS production might lead to lower efficiencies, it is more effective than the irradiation of the individual dyes, which can also be attributed to the high FRET efficiency from AO to RB. To again address a biological application and to estimate if the system can produce enough ROS to have an impact on a biological system, the very local toxic effect of the produced ROS was also evaluated on cancer cells. This scenario represents another challenge compared to antimicrobial resistance. While non-irradiated cells remained viable, cells that had been irradiated lost viability (see ESI,† Section S2.6). The cell experiments confirm that the amount of produced ROS is sufficient to affect cancer cells despite the potentially low reaction efficiency. This could be even more advantageous for highly localized treatments.

Tri-functionalized materials for two-photon excitation and small molecule release

Our ultimate goal was to combine the two previously mentioned functions to realize a material that is capable of releasing not only ROS, but also an additional active ingredient under 2-PE irradiation. This concept will benefit the conceptualization of future materials for highly localized synergistic therapy in deep tissue. A specific challenge of this application is the monitoring of the release, as it occurs highly localized only at irradiated particles in the focal volume. Assuming a focal volume of about one femtoliter (fl) and a particle size of 200 nm a detection method with upmost sensitivity is necessary. Therefore, we decided to leverage the use of a fluorescent probe and quantified its release *in situ* during two-photon microscopy. We replaced thymol which can only be quantified *via* GC-MS measurements, with an *in situ* detectable molecule that does not spectrally interfere with the optical properties of the FRET system (Fig. 4a and b). This was done without changing the oxolabile linker, which ensures the same release properties. Umbelliferone, a natural coumarin derivative is a suitable model drug for this purpose. The multifaceted and significant pharmacological properties of umbelliferone, including antioxidant, anti-inflammatory, and antimicrobial, render it a promising candidate for further drug development.[32]

MOPs-AO-RB-Umb were prepared, and characterization data are shown in the ESI,† Section S2.7. First, the occurrence of the free umbelliferone was determined under visible light radiation and confirmed by UV-VIS measurements, high-performance liquid chromatography (HPLC) and mass spectrometry; data are given in the ESI,† Section S2.8. Given that the focal volume of 2-PE lasers contains only one fl, diffusion out of the focus occurs rapidly, thereby presenting a challenge for *in situ* monitoring. To slow down particle and molecular diffusion, glycerol as a highly viscous liquid was chosen for monitoring umbelliferone release microscopically under 2-PE irradiation. ROS production as well as linker stability was not negatively affected by the change in solvent (see the ESI,† Section S2.9). The MOPs-AO-RB-Umb themselves could be detected due to their fluorescence and clearly showed the release of the essential oil molecule (Fig. 4c and Movie S2, ESI†). The presented data substantiate the postulated cascade reaction (Fig. 4a). To the best of our knowledge, this is the first time that the release of an antibacterial drug was detected *in situ* upon the ROS-triggered cleavage of an oxidative sensitive linker with 2-photon irradiation.

Conclusions

One of the primary challenges in targeted therapy is the precise and timed drug release of the desired drug, which is further complicated by the need to simultaneously release a second agent to enhance therapeutic effects. The coordination of dual-release systems requires the implementation of sophisticated advanced control mechanisms to guarantee the effective and synchronous delivery of both, thereby optimizing treatment efficacy while minimizing adverse effects. In this work, we present a novel approach for a radiation-triggered drug delivery system with a dual mechanism of action. Upon light irradiation, reactive oxygen species (ROS) are produced, which additionally initiate a cascade reaction that results in the release of a small molecule with beneficial properties in biomedical applications. To achieve this, we synthesized functionalizable MOPs, which were then covalently functionalized with Rose Bengal for ROS production. To release the small molecule, it was attached to the material *via* an oxolabile linker, which could be cleaved with the produced ROS. We focused on two applications using either linear or two-photon-based light excitation. Thymol, an alternative to antibiotics, was released using bi-functionalized particles and showed beneficial effects in the first antimicrobial experiments. By evolving our system to employ two-photon excitation, we could address the low penetration depth of light into tissue that limits the application

of light. For this purpose, FRET between Acridine Orange and Rose Bengal was used. The increased ROS production was monitored *in situ* microscopically. In a last and sophisticated experiment, we generated trifunctional particles that are equipped with an additional third fluorescent natural product (umbelliferone) and could, for the first time, monitor the *in situ* drug release from particles under two-photon irradiation. However, this concept is not confined to a single pharmaceutical agent – by simple molecular synthesis an array of small molecules for diverse applications could be released.

Data availability

The data supporting this article have been included as part of the ESI.†

Conflicts of interest

There are no conflicts to declare.

Acknowledgements

Part of the work was funded by the Deutsche Forschungsgemeinschaft (DFG, German Research Foundation) – SFB/TRR-298-SIIRI-Project 426335750. The authors thank Denis Pluta and Prof. Nadja Bigall for optoelectronic measurements. We thank Muhammad Imran Rahim for his support with the biological experiments and Gerald Dräger for the GC-MS measurements.

Notes and references

1 C. J. L. Murray, K. S. Ikuta, F. Sharara, L. Swetschinski, G. R. Aguilar, A. Gray, C. Han, C. Bisignano, P. Rao, E. Wool, S. C. Johnson, A. J. Browne, M. G. Chipeta, F. Fell, S. Hackett, G. Haines-Woodhouse, B. H. K. Hamadani, E. A. P. Kumaran, B. McManigal and M. Naghavi, *Lancet*, 2022, **399**, 629–655.
2 R. E. Kohman, S. S. Cha, H.-Y. Man and X. Han, *Nano Lett.*, 2016, **16**, 2781–2785.
3 Y. Liu, R. Qin, S. A. J. Zaat, E. Breukink and M. Heger, *J. Clin. Transl. Res.*, 2015, **1**, 140–167.
4 E. Polat and K. Kang, *Biomedicines*, 2021, **9**, 584.
5 X. Hu, H. Zhang, Y. Wang, B.-C. Shiu, J.-H. Lin, S. Zhang, C.-W. Lou and T.-T. Li, *Chem. Eng. J.*, 2022, **450**, 138129.
6 K. A. Hammer, C. F. Carson and T. V. Riley, *J. Appl. Microbiol.*, 1999, **86**, 985–990.
7 M. Cáceres, W. Hidalgo, E. Stashenko, R. Torres and C. Ortiz, *Antibiotics*, 2020, **9**, 147.
8 K. Kachur and Z. Suntres, *Crit. Rev. Food Sci. Nutr.*, 2020, **60**, 3042–3053.
9 M. Hyldgaard, T. Mygind and R. Meyer, *Front. Microbiol.*, 2012, 3.
10 A. Nostro, A. S. Roccaro, G. Bisignano, A. Marino, M. A. Cannatelli, F. C. Pizzimenti, P. L. Cioni, F. Procopio and A. R. Blanco, *J. Med. Microbiol.*, 2007, **56**, 519–523.
11 M. J. Darre, A. Kollanoor-Johny, K. Venkitanarayanan and I. Upadhyaya, *J. Appl. Poult. Res.*, 2014, **23**, 340–344.
12 C. Piombino, H. Lange, F. Sabuzi, P. Galloni, V. Conte and C. Crestini, *Molecules*, 2020, **25**, 866.
13 C. G. Dariva, J. F. J. Coelho and A. C. Serra, *J. Controlled Release*, 2019, **294**, 337–354.
14 A. Alabugin, *Photochem. Photobiol.*, 2019, **95**, 722–732.
15 F. Helmchen and W. Denk, *Nat. Methods*, 2005, **2**, 932–940.
16 M. Rubart, *Circ. Res.*, 2004, **95**, 1154–1166.
17 J. H. Strickler and W. W. Webb, *CAN-AM Eastern 90*, SPIE, 1991, pp. 107–118.
18 H. Bronner, F. Brunswig, D. Pluta, Y. Krysiak, N. Bigall, O. Plettenburg and S. Polarz, *ACS Appl. Mater. Interfaces*, 2023, **15**, 14067–14076.
19 J. Gehring, B. Trepka, N. Klinkenberg, H. Bronner, D. Schleheck and S. Polarz, *J. Am. Chem. Soc.*, 2016, **138**, 3076–3084.
20 A. Sharma, M.-G. Lee, M. Won, S. Koo, J. F. Arambula, J. L. Sessler, S.-G. Chi and J. S. Kim, *J. Am. Chem. Soc.*, 2019, **141**, 15611–15618.
21 J. Gehring, D. Schleheck, B. Trepka and S. Polarz, *ACS Appl. Mater. Interfaces*, 2015, **7**, 1021–1029.
22 H. Bronner, A.-K. Holzer, A. Finke, M. Kunkel, A. Marx, M. Leist and S. Polarz, *RSC Adv.*, 2020, **10**, 17327–17335.
23 S.-H. Cheng, C.-C. Hsieh, N.-T. Chen, C.-H. Chu, C.-M. Huang, P.-T. Chou, F.-G. Tseng, C.-S. Yang, C.-Y. Mou and L.-W. Lo, *Nano Today*, 2011, **6**, 552–563.
24 H. Liu, Y. Yang, A. Wang, M. Han, W. Cui and J. Li, *Adv. Funct. Mater.*, 2016, **26**, 2561–2570.
25 R. M. Clegg, *Laboratory Techniques in Biochemistry and Molecular Biology*, Elsevier, 2009, 1–57.
26 I. L. Medintz and N. Hildebrandt, *FRET - Förster Resonance Energy Transfer: From Theory to Applications*, John Wiley & Sons, 2013.
27 S. Vroom and D. Grauw Gerritsen, *J. Microsc.*, 1998, **191**, 39–51.
28 T. R. Neu, U. Kuhlicke and J. R. Lawrence, *Appl. Environ. Microbiol.*, 2002, **68**(2), 901–909.
29 F. Bestvater, E. Spiess, G. Stobrawa, M. Hacker, T. Feurer, T. Porwol, U. Berchner-Pfannschmidt, C. Wotzlaw and H. Acker, *J. Microsc.*, 2002, **208**, 108–115.
30 J. James, N. Fiji, D. Roy, D. A. Mg, M. Sham Shihabudeen, D. Chattopadhyay and K. Thirumurugan, *Anal. Methods*, 2015, **7**, 8572–8575.
31 E. Eruslanov and S. Kusmartsev, *Advanced Protocols in Oxidative Stress II*, D. Armstrong, Humana Press, Totowa, NJ, 2010, pp. 57–72.
32 O. Mazimba, *Bull. Fac. Pharm.*, 2017, **55**, 223–232.

